Parity chain and parity chain breaking in the two-level cavity quantum electrodynamics system

Jingyun Zhao (赵晶云)[1,2,4], Liguo Qin (秦立国)[2,3,*], Xunming Cai (蔡勋明)[1], Qiang Lin (林 强)[1,5], and Zhongyang Wang (王中阳)[2,]**

[1]*Institute of Optics, Department of Physics, Zhejiang University, Hangzhou 310027, China*
[2]*Shanghai Advanced Research Institute, Chinese Academy of Sciences, Shanghai 201210, China*
[3]*School of Science, Qingdao University of Technology, Qingdao 266000, China*
[4]*School of Science, Zhejiang Sci.-Tech. University, Hangzhou 310018, China*
[5]*Department of Applied Physics, Zhejiang University of Technology, Hangzhou 310023, China*
**Corresponding author: lgqin@foxmail.com; **corresponding author: wangzy@sari.ac.cn*
Received November 2, 2016; accepted February 10, 2017; posted online March 2, 2017

We investigate the transitions between energy levels and parity symmetry in an effective two-level polar molecule system strongly coupled with a quantized harmonic oscillator. By the dressed-state perturbation theory, the transition diagrams between the dressed-state energy levels are presented clearly and show that the odd (even) parity symmetry is broken by the permanent dipole moment (PDM) of the polar molecules. By the analytical and numerical methods, we find that when the coupling strength and the PDM increase, the more frequency components are induced by the counter-rotating terms and PDM.

OCIS codes: 020.5580, 140.3945, 270.0270.
doi: 10.3788/COL201715.050202.

As one of the simplest models that deals with the matter–light interaction, an effective two-level quantum system can be coupled with a quantized harmonic oscillator. This ubiquitous model is applied to a great variety of physical systems, ranging from quantum optics to quantum information, such as circuit and cavity quantum electrodynamics (QED)[1–6]. One of the most well-known is the quantum Rabi model[7,8], which can be reduced to solvable dynamics called the Jaynes–Cummings (JC) model[9,10] in the rotating wave approximation (RWA), where the counter-rotating terms (CRTs) are ignored[11]. The RWA is valid when the coupling strength λ between the two-level system and the cavity field is far smaller than the cavity field frequency ω_c and the transition frequency ω_0 of the two-level system[12]. The JC model possesses a continuous $U(1)$ symmetry, however, which is broken down to $\mathbb{Z}_2$ (the Abelian group) in the Rabi model due to the presence of the CRT[13]. This $\mathbb{Z}_2$ symmetry, usually called parity, generates the linear combinations of quantum states such that they are either an even or an odd parity[13], the eigenvalues of whose operator are ± 1. The parity symmetry of the model is useful for understanding how its dynamics evolve inside the Hilbert space[14]. In the Rabi model of the cavity QED, the quantum states of the system can be split into two unconnected subspaces or parity chains. Neighboring states within each parity chain can be connected via the CRT [or rotating terms (RTs)][15]. However, this parity symmetry can be broken, such as the local bias fields[16] or the Ising interaction[17].

Recent progresses draw the extensive attention to the ultrastrong-coupling (USC) regime in the superconducting circuit cavity QED with the normalized coupling strength λ/ω_c reaching 0.1[18,19], where the CRT of the interaction is no longer ignored and induces the Bloch–Siegert (B-S) shift, and the population dynamics no longer show strictly periodic Rabi oscillation, but complicated chaotic behavior instead[20–22]. Moreover, in the strong-coupling regime, we have demonstrated that the permanent dipole moment (PDM) term comparable with the CRT cannot be neglected in the molecule–cavity coupling system[23]. In the USC regime, the parity symmetry shows the advantage in the aspect of the generation and reconstruction of arbitrary states[24]. Recently, Garziano *et al.*[25] studied a quantum circuit constituted by a coplanar resonator interacting with a number of flux qubits in the USC regime and found that the parity symmetry of a qubit (an artificial atom) with an even potential is broken by the interaction with a resonator field displaying a nonzero vacuum (ground–state) expectation value.

Nowadays, the strong-coupling regime has also been reached in the molecule coupled with a microcavity, especially the organic molecule microcavity[26]. Control of molecular excitation during the plasma generation of a femtosecond laser pulse has been reported[27]. The polar molecule–cavity coupling system includes the RT, CRT, and PDM term. As a unique property of the polar molecule, the PDM has been studied and measured experimentally[28]. The effects of both the PDM and CRT on the energy level and stationary state wave function of the system have been studied in our earlier work[23]. In this Letter, based on the dressed-state perturbation theory, we study the effects of the CRT and PDM terms on the transitions between dressed-state energy levels, the parity symmetry, and the dynamical evolution of a two-level cavity QED system beyond the RWA. The results

show that the CRT induces the transitions within an independent parity chain, while the transitions between the two parity chains are induced by the PDM term. Therefore, for the polar molecule, the parity symmetry is broken by the PDM term. In addition, we analyze the frequency components of the transitions among more dressed states induced by the CRT and PDM terms, and show that the population evolution contains more oscillatory frequencies, not just the single Rabi frequency of the JC model within the RWA. We believe that our results will be helpful for further understanding the cavity QED in the regime of the polar molecule–light interaction.

The system we consider here is an effective two-level quantum system coupled with a quantized cavity field. The two-level system can be a single atom ($\alpha = 0$) or molecule ($\alpha \neq 0$) with the ground and first excited states. The Hamiltonian can be described by[29]

$$H = \omega_c a^\dagger a + \frac{1}{2}\omega_0 \sigma_z - \lambda(\alpha\sigma_z + \sigma_x)(a^\dagger + a), \tag{1}$$

where a ($a^\dagger$) is the annihilation (creation) operator of the single-mode bosonic field, $\sigma_{x,z}$ are the usual Pauli spin operators, λ is the coupling strength, $\alpha = \frac{\mu_{ee}-\mu_{gg}}{2\mu_{ge}}$ is the normalized permanent dipole difference with the dipole moment $\mu_{\mu\nu}$ $(\mu, \nu = g, e)$[30–32], and for simplicity, here we have already set the unit $\hbar = 1$. The model describes a polar molecule–cavity coupling system, which can be reduced to the Rabi model for $\alpha = 0$ or the JC model with $\alpha = 0$ and the RWA.

According to the Schrödinger equation and the dressed-state perturbation theory, where the interaction Hamiltonian of both the PDM and the CRT are viewed as a perturbation term[23], we have obtained the analytical energy levels $E_{g,0}$, $E_n^\pm$ and the wave function $|\Psi_{g,0}\rangle$, $|\Psi_n^\pm\rangle$ of the ground state and excited states in the perturbation case, where $|\Psi_n^\pm\rangle$ $(E_n^\pm)$ is the summation of the zero-order perturbation term $|\psi_n^\pm\rangle$ $(\varepsilon_n^\pm)$ and the kth-order perturbation term $|\psi_n^{\pm(k)}\rangle$ $(\varepsilon_n^{\pm(k)})$. By comparison, we have found that the perturbation results are in good agreement with the numerical simulation in the steady state[23]. Here, the system is initially prepared in its excited state, and the cavity field is in the vacuum state, *i.e.*, $|\Psi(0)\rangle = |e, 0\rangle$. By using the eigenvectors and eigenvalues, the dynamical wave function of the Hamiltonian [Eq. (1)] can be expressed as

$$|\Psi(t)\rangle = Ce^{-iE_{g,0}t}|\Psi_{g,0}\rangle + \sum_{k=0}^{\infty}(A_k e^{-iE_k^+ t}|\Psi_k^+\rangle + B_k e^{-iE_k^- t}|\Psi_k^-\rangle), \tag{2}$$

where the expressions of $E_{g,0}$, $|\Psi_{g,0}\rangle$, $E_k^\pm$ and $|\Psi_k^\pm\rangle$ can be calculated and found in Ref. [23]. To simplify the problem concerned, here we consider the wave function up to the first-order perturbation and the energy up to the second-order perturbation. The coefficients $C = \langle\Psi_{g,0}|\Psi(0)\rangle$, $A_k = \langle\Psi_k^+|\Psi(0)\rangle$, and $B_k = \langle\Psi_k^-|\Psi(0)\rangle$ $(k = 0, 1, 2)$ can be found in Ref. [23] and satisfy the normalization condition. For the validity of the dressed-state perturbation theory, the parameters used here should satisfy the conditions of the perturbation. Therefore, the matrix element of the perturbation operator between the perturbing state $|\varphi_n^\pm\rangle$ and the unperturbed state $|\varphi_k^\pm\rangle$ should be much smaller than the energy difference between the two states: $\left|\frac{V_{nk}^{\pm\pm}}{\varepsilon_n^\pm - \varepsilon_k^\pm}\right| \ll 1$[23]. Thus, the power series of E and $|\Psi\rangle$ will converge quickly. Through calculation, our theory of up to a second-order correction is valid in a certain range of both the normalized coupling strength $f = \lambda/\omega_c$ and the α value, where $f \ll 0.4$, $\alpha \ll \frac{2}{(2+\sqrt{3})f} - 2$ in the resonant case, and the range of validity of α narrows as the f value increases.

Using the explicit form of wave functions, we can obtain the population difference at an arbitrary time t as

$$\begin{aligned}\langle\sigma_z(t)\rangle = {} & D_{n0g0}\cos[(E_0^- - E_{g,0})t] \\ & + D_{p0g0}\cos[(E_0^+ - E_{g,0})t] + D_{n1g0}\cos[(E_1^- - E_{g,0})t] \\ & + D_{p1g0}\cos[(E_1^+ - E_{g,0})t] + D_{n2g0}\cos[(E_2^- - E_{g,0})t] \\ & + D_{p2g0}\cos[(E_2^+ - E_{g,0})t] + D_{p0n0}\cos[(E_0^+ - E_0^-)t] \\ & + D_{n1n0}\cos[(E_1^- - E_0^-)t] + D_{p1n0}\cos[(E_1^+ - E_0^-)t] \\ & + D_{n2n0}\cos[(E_2^- - E_0^-)t] + D_{p2n0}\cos[(E_2^+ - E_0^-)t] \\ & + D_{n1p0}\cos[(E_1^- - E_0^+)t] + D_{p1p0}\cos[(E_1^+ - E_0^+)t] \\ & + D_{n2p0}\cos[(E_2^- - E_0^+)t] + D_{p2p0}\cos[(E_2^+ - E_0^+)t] \\ & + D_{p1n1}\cos[(E_1^+ - E_1^-)t] + D_{n2n1}\cos[(E_2^- - E_1^-)t] \\ & + D_{p2n1}\cos[(E_2^+ - E_1^-)t] + D_{n2p1}\cos[(E_2^- - E_1^+)t] \\ & + D_{p2p1}\cos[(E_2^+ - E_1^+)t] + D_{p2n2}\cos[(E_2^+ - E_2^-)t],\end{aligned} \tag{3}$$

where the subscripts of the coefficients $j = n, p$ are labeled "−" and "+", respectively. The different coefficients $D_{jkj'k'}$ with the different subscripts represent the probability amplitudes of the transitions between the various perturbed energy levels. Eq. (3) shows the 21 different transitions with the 21 different frequencies, which are graphically plotted in Fig. 1.

From Ref. [15], we know that the system dynamics inside the Hilbert space can split into two unconnected subspaces or parity chains consisting of the dressed states. By using the parity chains, here we plot the transitions between the perturbed dressed states in Fig. 2, where the transitions caused by RT, CRT, and PDM are labeled. It is worth noting that the transitions caused by RT only exist between $|\varphi_{2j}^+\rangle$ and $|\varphi_{2j}^-\rangle$ $(j = 0, 1, 2, ...)$, whereas the CRT can induce the transitions between the neighboring states in the single parity chain and cannot cause the transitions between the two states in two different parity chains. More importantly, the PDM can lead to the transitions between the two different parity chains, *i.e.*, the two unconnected parity chains are connected by the PDM. Therefore, the parity symmetry is conserved in

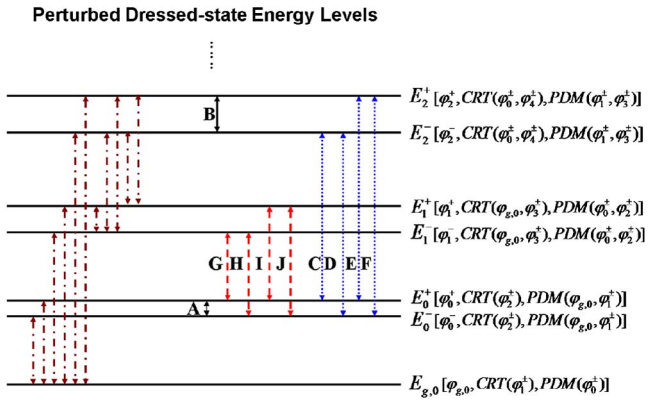

Fig. 1. Transitions between the perturbed energy levels with the first-order perturbed dressed states. The three terms in the parentheses on the right side of the figure separately represent the unperturbed dressed state and the dressed states caused by the CRT and PDM. The arrows represent the 21 frequency components, where the main probability transitions are labeled by the alphabet "A, B, ..., J".

the JC and Rabi models, however, they are broken in the polar molecule–cavity coupling model. This point is an important result of our work. In the following, we will analyze the frequencies in the these transitions.

The transition frequency comes from the difference between both energy levels, hence, we will study these transitions by the population inversion of the two-level. Initially, when the quantum field is in the Fock state and the two-level system with $\alpha = 0$ is in the excited state, it is well-known that in the limit of the JC model the population inversion of the two-level system shows strictly periodic Rabi oscillation, whose Rabi frequency $\Omega_{n\delta} = \sqrt{\delta^2 + 4\lambda^2(n+1)}$ depends on the photon number n of the initial cavity field and the detuning $\delta = \omega_0 - \omega_c$[33]. In the strong-coupling case, the population dynamics of the Rabi model beyond the RWA has also been theoretically studied and shows that the structure of the Rabi oscillations is greatly modified[20]. Yet, the effects of the CRT and PDM on the dynamical evolution of the population are not clearly given to the best of our knowledge. Here, based on the dressed-state perturbation theory, taking into account the contributions of both the CRT and PDM, we not only find more oscillating frequencies in the population difference, but it also clearly shows the transition relations between the dressed states.

The population difference $\langle\sigma_z(t)\rangle$ is calculated and plotted in Fig. 3 for $f = \lambda/\omega_c = 0.01, 0.1$ with the different α. By comparison, we find that the analytical results agree quite well with the numerical ones within the applicable regime of the perturbation theory for the different f and α. When α increases beyond the perturbation regime, the analytical results begin to gradually deviate from the numerical ones for the long time scale. It is worth noting that the valid regime of α becomes narrow, as the coupling strength f increases in the perturbation regime, as in the previous discussions. Apparently, the dressed-state perturbation theory can give the appropriate dynamics in the coupling regime $\lambda < 0.1\omega_c$ and the normalized permanent dipole difference $\alpha < 1$.

In the case of the polar molecule with $\alpha \neq 0$, the population inversion shows similar behavior in the Rabi type ($\alpha = 0$) oscillation, as shown in Fig. 3, however, it actually contains more oscillatory frequencies than those in the case of $\alpha = 0$ due to the effects of the PDM. In Fig. 4, we give the analysis of the frequency components in the transitions based on the Fourier transform of the population difference $\langle\sigma_z(t)\rangle$ by both the analytic and numerical methods.

In the case of the two-level atom Rabi model, where the CRT induces the transition along two independent parity chains of the Hilbert space (as shown in Fig. 2) coincident with the result of Ref. [15], there are six frequency components induced by the RT and CRT altogether. While in the polar molecule case, the parity symmetry is broken by the PDM[34], *i.e.*, the two parity chains initially independent in the two-level atom Rabi model are now coupled together by the PDM. The involvement of the PDM terms will cause the transitions among the more dressed states, such as $|\varphi_0^{\pm}\rangle \leftrightarrow |\varphi_{g,0}\rangle$, $|\varphi_0^{\pm}\rangle \leftrightarrow |\varphi_1^{\pm}\rangle$, and $|\varphi_1^{\pm}\rangle \leftrightarrow |\varphi_2^{\pm}\rangle$, as shown

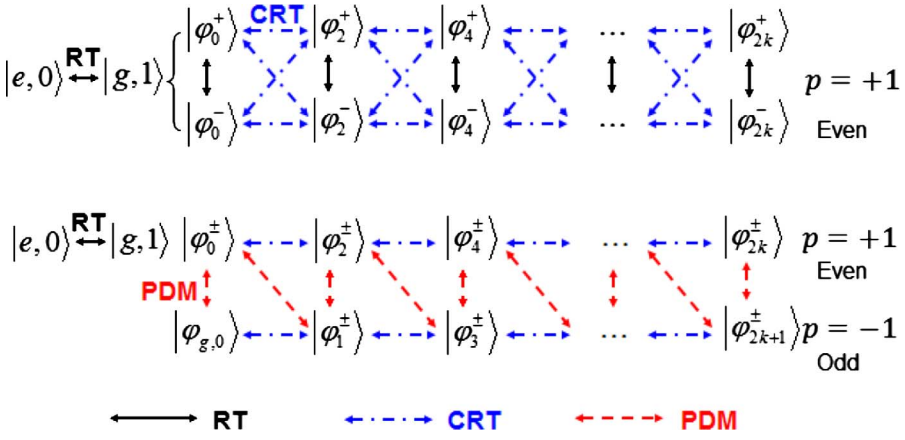

Fig. 2. Transitions between the dressed-state energy levels caused by the RT, CRT and, PDM in the parity chains, respectively. The initial state of the system starts is $|e,0\rangle$.

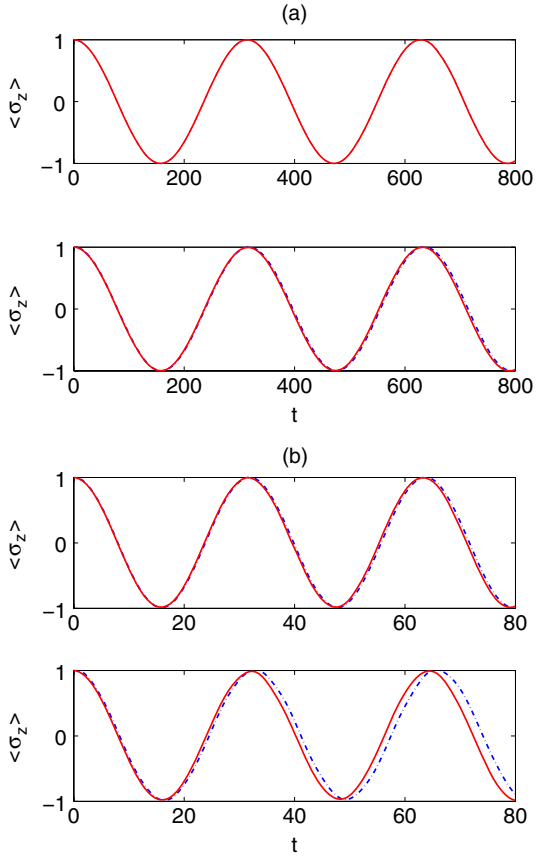

Fig. 3. Population differences $\langle\sigma_z(t)\rangle$ at the resonant case for different normalized coupling strengths $f=\lambda/\omega_c$ with different normalized permanent dipole difference α. (a) $f=0.01$, $\alpha=1,5$ (from top to bottom). (b) $f=0.1$, $\alpha=0.5,1$ (from top to bottom). Our dressed-state perturbation theory (blue dot–dashed lines) are compared with the numerical simulation results (red solid lines).

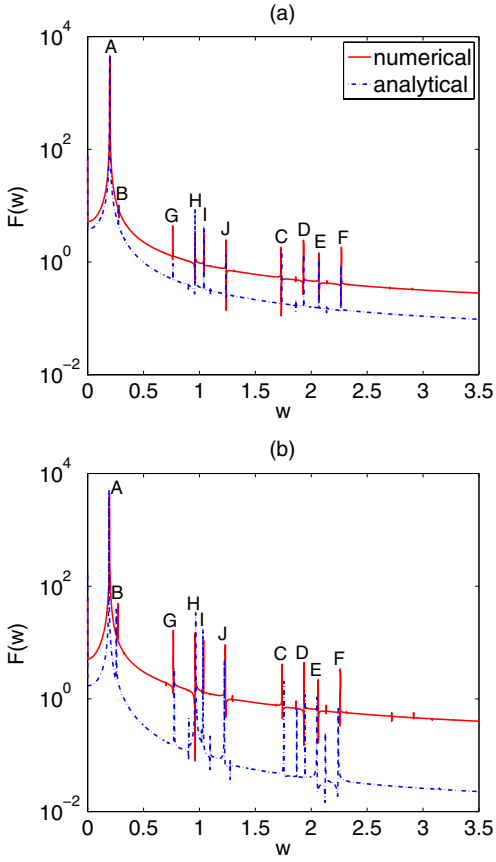

Fig. 4. Fourier transform of the population difference at the resonance for different normalized permanent dipole difference α with $\lambda=0.1\omega_c$. (a) $\alpha=0.5$; (b) $\alpha=1$. The ten frequency peaks A, B, C, D, E, F, G, H, I, and J correspond to the transitions between the perturbed energy levels in Fig. 1. Our dressed-state perturbation theory (blue dot–dashed lines) are compared to the numerical simulation results (red solid lines).

in Fig. 2. In the regime of the perturbation theory we consider that 15 frequency components are introduced additionally due to the PDM, *i.e.*, $E_1^{\pm}-E_0^{\pm}$, $E_1^{+}-E_1^{-}$, $E_0^{\pm}-E_{g,0}$, $E_1^{\pm}-E_{g,0}$, $E_2^{\pm}-E_1^{\pm}$, $E_2^{\pm}-E_{g,0}$. There are 21 components induced by the RT, CRT, and PDM altogether, as shown in Figs. 1 and 4(a). Yet, due to far less proportions of higher-order dressed states, not all of them are shown clearly in Fig. 4. It is observed that the dominating frequency is still $E_0^{+}-E_0^{-}$ (frequency peak A), however, the small peaks of $E_1^{+}-E_1^{-}$ and $E_2^{+}-E_2^{-}$ (labeled by B) on the right side of peak A (the transition $E_0^{+}-E_0^{-}$) are still too small to be submerged. There are ten frequency peaks around $w=1$, among which four of the second-highest frequencies are $E_1^{-}-E_0^{+}$, $E_1^{-}-E_0^{-}$, $E_1^{+}-E_0^{+}$, and $E_1^{+}-E_0^{-}$, corresponding to the frequency peaks G, H, I, and J from left to right, and the other six frequency peaks $E_2^{-}-E_1^{+}$, $E_0^{-}-E_{g,0}$, $E_2^{-}-E_1^{-}$, $E_2^{+}-E_1^{+}$, $E_0^{+}-E_{g,0}$, and $E_2^{+}-E_1^{-}$ are too small to be distinguished. There are six frequency peaks around $w=2$, among which four of the second-highest frequencies are $E_2^{-}-E_0^{+}$, $E_2^{-}-E_0^{-}$, $E_2^{+}-E_0^{+}$, and $E_2^{+}-E_0^{-}$, corresponding to frequency peaks C, D, E, and F from left to right, and the other two frequency peaks $E_1^{-}-E_{g,0}$ and $E_1^{+}-E_{g,0}$ are too small to be distinguished. The two small frequency peaks around $w=3$ are $E_2^{\pm}-E_{g,0}$.

For the polar molecule–cavity QED, the transition relations among dressed states are different with the case of the atom cavity QED ($\alpha=0$) due to the effect of the PDM. Taking the dominating frequency $E_0^{+}-E_0^{-}$ as an example, the state of E_0^{+} is composed of $|\varphi_0^{+}\rangle$, $|\varphi_2^{\pm}\rangle$, $|\varphi_{g,0}\rangle$ and $|\varphi_1^{\pm}\rangle$ (where $|\varphi_0^{+}\rangle$ is dominant, $|\varphi_2^{\pm}\rangle$ comes from the perturbation of the CRT, and $|\varphi_{g,0}\rangle$, $|\varphi_1^{\pm}\rangle$ come from the perturbation of the PDM), as shown in Fig. 1, while the state of E_0^{-} is composed of $|\varphi_0^{-}\rangle$, $|\varphi_2^{\pm}\rangle$, $|\varphi_{g,0}\rangle$ and $|\varphi_1^{\pm}\rangle$ (where $|\varphi_0^{-}\rangle$ is dominant, $|\varphi_2^{\pm}\rangle$ comes from the perturbation of the CRT, and $|\varphi_{g,0}\rangle$, $|\varphi_1^{\pm}\rangle$ come from the perturbation of the PDM). So, the frequency peak $E_0^{+}-E_0^{-}$ mainly comes from the transition $|\varphi_0^{+}\rangle\leftrightarrow|\varphi_0^{-}\rangle$, which is dominant and caused by the RT interaction. Besides, the frequency peak $E_0^{+}-E_0^{-}$ also includes the transition $|\varphi_0^{\pm}\rangle\leftrightarrow|\varphi_{g,0}\rangle$, $|\varphi_1^{\pm}\rangle$, $|\varphi_2^{\pm}\rangle$ and $|\varphi_1^{\pm}\rangle\leftrightarrow|\varphi_{g,0}\rangle$, $|\varphi_2^{\pm}\rangle$, as shown in Fig. 2. Then, taking another frequency peak $E_1^{-}-E_0^{+}$ as another example, the state of E_1^{-} is composed of $|\varphi_1^{-}\rangle$, $|\varphi_{g,0}\rangle$, $|\varphi_3^{\pm}\rangle$, $|\varphi_0^{\pm}\rangle$ and $|\varphi_2^{\pm}\rangle$ (where $|\varphi_1^{-}\rangle$ is dominant, $|\varphi_{g,0}\rangle$, $|\varphi_3^{\pm}\rangle$ come from

the perturbation of the CRT, and $|\varphi_0^{\pm}\rangle$, $|\varphi_2^{\pm}\rangle$ come from the perturbation of the PDM), so the frequency peak $E_1^- - E_0^+$ mainly comes from the transition $|\varphi_1^-\rangle \leftrightarrow |\varphi_0^+\rangle$, which has far less proportion because it is caused by the perturbation of the PDM. Besides, the frequency peak $E_1^- - E_0^+$ also includes the transition $|\varphi_0^{\pm}\rangle \leftrightarrow |\varphi_{g,0}\rangle$, $|\varphi_1^{\pm}\rangle$, $|\varphi_2^{\pm}\rangle$ and $|\varphi_1^{\pm}\rangle \leftrightarrow |\varphi_{g,0}\rangle$, $|\varphi_2^{\pm}\rangle$, $|\varphi_1^{\pm}\rangle$, $|\varphi_2^{\pm}\rangle \leftrightarrow |\varphi_3^{\pm}\rangle$, $|\varphi_0^-\rangle \leftrightarrow |\varphi_0^+\rangle$, $|\varphi_1^-\rangle \leftrightarrow |\varphi_1^+\rangle$, and $|\varphi_2^-\rangle \leftrightarrow |\varphi_2^+\rangle$, as shown in Fig. 2. We can obtain the transition relations among the dressed states included theoretically in the 21 frequency peaks. It is expected from Fig. 4(b) that when the α value increases beyond the valid regime of the perturbation theory, the more frequency components will appear, which correspond to the transitions between higher dressed-state energy levels.

In conclusion, we investigate the symmetry and its breaking of the parity chains in an effective two-level molecule–cavity QED system by the dressed-state perturbation theory. We find that the RT and CRT do not disturb the parity symmetry, whereas, the PDM can break the parity symmetry and bridge a transition between the even and odd parity chains. Because of the effects of the RT, CRT, and PDM, more frequency components are induced into the Rabi frequency, which is modified, and not the strict Rabi oscillation, as shown in the JC model within the RWA. In the frequency domain of the Fourier transform, we find that more induced frequencies appear as the coupling strength and the PDM increase. In addition, we give the clear transition diagram and one-to-one correspondence between the frequency and the transition, which is helpful for further understanding the cavity QED in the regime of the atom and molecule–light interaction.

This work was supported by the National Natural Sciences Foundation of China (Nos. 61605225, 11547035, 11505100, and 61475139), the Natural Science Foundation of Shanghai (No. 16ZR1448400), the Strategic Priority Research Program of the Chinese Academy of Sciences (No. XDB01010200), the Hundred Talents Program of the Chinese Academy of Sciences (No. Y321311401), the National 973 Program of China (No. 2013CB329501), the Shandong Provincial Natural Science Foundation (No. ZR2015AQ007), and the Zhejiang Provincial Natural Science Foundation (No. LQ13A040006).

References

1. J. M. Raimond, M. Brune, and S. Haroche, Rev. Mod. Phys. **73**, 565 (2001).
2. M. Brune, F. Schmidt-Kaler, A. Maali, J. Dreyer, E. Hagley, J. M. Raimond, and S. Haroche, Phys. Rev. Lett. **76**, 1800 (1996).
3. H. Mabuchi and A. C. Doherty, Science **298**, 1372 (2002).
4. D. Esteve, J. M. Raimond, and J. Dalibard, *Quantum Entanglement and Information Processing* (Elsevier, 2004).
5. I. Chiorescu, P. Bertet, K. Semba, Y. Nakamura, C. J. P. M. Harmans, and J. E. Mooij, Nature **431**, 159 (2004).
6. X. Zhong, G. Lin, F. Zhou, Y. Niu, and S. Gong, Chin. Opt. Lett. **13**, 092701 (2015).
7. I. I. Rabi, Phys. Rev. **49**, 324 (1936).
8. I. I. Rabi, Phys. Rev. **51**, 652 (1937).
9. E. T. Jaynes and F. W. Cummings, Proc. IEEE **51**, 89 (1963).
10. B. W. Shore and P. L. Knight, J. Mod. Opt. **40**, 1195 (1993).
11. M. O. Scully and M. S. Zubairy, *Quantum Optics* (Cambridge University, 1997).
12. E. K. Irish, Phys. Rev. Lett. **99**, 173601 (2007).
13. D. Braak, Phys. Rev. Lett. **107**, 100401 (2011).
14. H. Wang, D. Ling, G. Chen, and X. Zhu, Chin. Opt. Lett. **13**, 011901 (2015).
15. J. Casanova, G. Romero, I. Lizuain, J. J. Garca-Ripoll, and E. Solano, Phys. Rev. Lett. **105**, 263603 (2010).
16. T. Liu, M. Feng, W. L. Yang, J. H. Zou, L. Li, Y. X. Fan, and K. L. Wang, Phys. Rev. A **88**, 013820 (2013).
17. Q. Wang, Z. He, and C. M. Yao, Commun. Theor. Phys. **63**, 510 (2015).
18. P. Forn-Díaz, J. Lisenfeld, D. Marcos, J. J. García-Ripoll, E. Solano, C. J. P. M. Harmans, and J. E. Mooij, Phys. Rev. Lett. **105**, 237001 (2010).
19. T. Niemczyk, F. Deppe, H. Huebl, E. P. Menzel, F. Hocke, M. J. Schwarz, J. J. Garcia-Ripoll, D. Zueco, T. Hümmer, E. Solano, A. Marx, and R. Gross, Nat. Phys. **6**, 772 (2010).
20. J. Larson, Phys. Scr. **76**, 146 (2007).
21. A. Pereverzev and E. R. Bittner, Phys. Chem. Chem. Phys. **8**, 1378 (2006).
22. C. J. Gan and H. Zheng, Eur. Phys. J. D **59**, 473 (2010).
23. J. Y. Zhao, L. G. Qin, X. M. Cai, Q. Lin, and Z. Y. Wang, Chin. Phys. B **25**, 044202 (2016).
24. S. Felicetti, T. Douce, G. Romero, P. Milman, and E. Solano, Sci. Rep. **5**, 11818 (2015).
25. L. Garziano, R. Stassi, A. Ridolfo, O. Di Stefano, and S. Savasta, Phys. Rev. A **90**, 043817 (2014).
26. J. R. Tischler, M. S. Bradley, V. Bulović, J. H. Song, and A. Nurmikko, Phys. Rev. Lett. **95**, 036401 (2005).
27. Q. Wang, Y. Zhang, Z. Wang, J. Ding, Z. Liu, and B. Hu, Chin. Opt. Lett. **14**, 110201 (2016).
28. B. Graner, Y. Chen, E. G. Lindahl, and B. R. Heckel, Phys. Rev. Lett. **116**, 161601 (2016).
29. T. Hattori and T. Kobayashi, Phys. Rev. A **35**, 2733 (1987).
30. P. J. Dagdigian, H. W. Cruse, and R. N. Zare, J. Chem. Phys. **60**, 2330 (1974).
31. A. R. Allouche, G. Wannous, and M. Aubert-Frécon, Chem. Phys. **170**, 11 (1993).
32. S. H. Nilar, A. J. Thakkar, A. E. Kondo, and W. J. Meath, Can. J. Chem. **71**, 1663 (1993).
33. B. W. Shore and P. L. Knight, J. Mod. Opt. **40**, 1195 (1993).
34. S. He, Y. Y. Zhang, Q. H. Chen, X. Z. Ren, T. Liu, and K. L. Wang, Chin. Phys. B **22**, 064205 (2013).